Int. J. Solids Structures, 1971, Vol. 7, pp. 1505 to 1522. Pergamon Press. Printed in Great Britain

FLEXURAL PULSE PROPAGATION IN NONUNIFORM ELASTIC BARS BY GEOMETRIC ACOUSTICS

D. RADER and M. MAO

Department of Engineering and Applied Science, Yale University, New Haven, Connecticut

Abstract—A direct numerical procedure is developed for analyzing the refraction of a flexural wave which impinges on a finite region of variable mechanical impedance in an elastic bar. This region is approximated by a set of uniform impedance elements, regarded as Timoshenko beams, to which the methods of geometric acoustics are applied. The analysis is performed for an infinite harmonic wave train and is extended to the case of a pulse by means of numerical Fourier synthesis. Numerical results are obtained for several examples in which experiments were performed and the calculated pulses are in close agreement with those observed experimentally. It is found that the contribution of the continuing interaction between propagating and nonpropagating waves accumulates within a nonuniform region and can significantly affect the net pulses of transmission and reflection.

1. INTRODUCTION

IN A previous paper [1], the authors investigated the reflection and transmission of longitudinal stress pulses which were incident on a finite region of variable mechanical impedance in a bar. It was found that when such a region is approximated by a set of uniform impedance steps, the refraction problem could be satisfactorily treated using geometric acoustics, i.e. the mechanical analogue of geometric optics. In the present work we consider the corresponding problem for flexural pulse propagation using an extension of this technique.

Several authors, e.g. Tyutekin and Shkvarnikov [2, 3] and Pierce [4], have discussed the use of the WKBJ (after Wentzel, Kramers, Brillouin and Jeffreys) approximation in dealing with wave propagation and vibration problems in nonuniform, inhomogeneous bars and plates. The WKBJ approximation can be used when the coefficients of the governing differential equation of motion are slowly varying functions of position. Physically, this corresponds to slowly varying mechanical and geometric properties in relation to some typical wavelength. The present approach, however, is not restrictive in this sense. It is required only that the physical assumptions underlying the governing equation of motion remain valid.

The analysis in this paper is concerned with the propagation of a flexural pulse along a circular elastic bar consisting of two uniform and homogeneous end sections connected by a transition region of variable diameter and mechanical properties. A flexural pulse which propagates along one of the end sections of such a bar, and impinges on the transition region, will give rise to refracted pulses of reflection and transmission. In order to calculate these pulses the transition region is first approximated by a number of uniform and homogeneous impedance elements. At the junction between elements there may be a discontinuity in area and mechanical properties (elastic moduli and density). Refraction coefficients are deduced for a single discontinuity and are used at each successive one along selected trajectories through the transition. This is done for each relevant harmonic in the Fourier

spectrum of the incident pulse and the refracted pulses are calculated by numerical Fourier synthesis with a digital computer.

The reflection and transmission of a flexural wave at an area jump in a homogeneous elastic bar was investigated by Mugiono [5] and by Ripperger and Abramson [6] within the framework of Euler–Bernoulli beam theory. The basic analysis in [5, 6] is employed in this paper except that the bars are treated as Timoshenko beams. The solution to the refraction problem for a Timoshenko beam is valid over a wider range of frequencies than could be expected from the elementary theory. This extended range of validity is essential in studying the propagation of a pulse for which the Fourier spectrum is rich in relatively high frequency components [7]. In the present work it is convenient, however, to consider frequencies no higher than that corresponding to pure thickness-shear vibrations of a Timoshenko beam. This restricted frequency range is still well beyond the useful range of Euler–Bernoulli theory. The highest significant frequencies associated with the experimental pulses were also less than the pure thickness-shear frequency so that experiment and analysis were compatible.

In the case of non-dispersive longitudinal pulse propagation through a nonuniform elastic region [1], the refraction coefficients relating the amplitudes of the incident, reflected and transmitted pulses at each impedance jump are constants which depend only on the cross sectional areas and material properties of neighboring elements. In the flexural problem, however, the refraction coefficients are also functions of frequency. Moreover, an incident flexural harmonic wave gives rise to both propagating waves and exponentially decaying standing or "non-propagating" waves at each impedance jump. Similarly, an incident standing wave gives rise to both types of waves. The cumulative interaction of harmonic and standing waves is found to contribute significantly to the net refracted pulses for the transition region as a whole.

Experiments are performed with homogeneous circular aluminum bars having conical transition regions. Calculated and experimental results for the refracted pulses are found to be in good agreement.

2. ANALYSIS

2.1 *Uniform Timoshenko beam*

The equation of motion of a Timoshenko beam [8] can be written in the form

$$c_0^2\kappa^2\frac{\partial^4 y}{\partial x^4}+\frac{\partial^2 y}{\partial t^2}-\kappa^2\left(1+\frac{E}{\lambda\mu}\right)\frac{\partial^4 y}{\partial x^2\partial t^2}+\frac{\kappa^2}{\lambda c_2^2}\frac{\partial^4 y}{\partial t^4}=0 \tag{1}$$

where x is the coordinate along the beam axis, t is the time, y is the transverse velocity, E is Young's modulus, μ is the shear modulus, κ is the radius of gyration of the cross section, c_2 is the velocity of pure distortional waves in unbounded media, c_0 is the velocity of extensional waves of long wavelength in a bar [$c_2=(\mu/\rho)^{\frac{1}{2}}$ and $c_0=(E/\rho)^{\frac{1}{2}}$, where ρ is the density] and λ is the ratio of the average shear stress to the maximum shear stress through the cross section in static bending. In particular, for a circular bar one has $\lambda=0{\cdot}75$. The appropriateness of using the static value of λ in the dynamic problem is discussed below.

A solution to (1) for a sinusoidal wave of angular frequency ω is

$$y=\{A_1\exp(ir_1x)+A_2\exp(ir_2x)+A_3\exp(ir_3x)+A_4\exp(ir_4x)\}\exp(i\omega t) \tag{2}$$

where A_1, A_2, A_3, A_4 are constants and the wave numbers r_1, r_2, r_3, r_4 are the four distinct roots of the frequency equation

$$r = \pm[b_1 \pm (b_1^2 - b_2)^{\frac{1}{2}}]^{\frac{1}{2}} \tag{3}$$

and

$$b_1 = \frac{\omega^2}{2c_0^2}\left(1 + \frac{E}{\lambda\mu}\right), \quad b_2 = \frac{\omega^2}{c_0^2\kappa^2}\left(\frac{\kappa^2\omega^2}{\lambda c_2^2} - 1\right). \tag{4}$$

For isotropic elastic materials, such as the aluminum bars used in the present work, one always has $b_1^2 - b_2 > 0$ in (3). Equation (3) is plotted nondimensionally in Fig. 1 for a circular aluminum bar in the form $\omega a/c_2$ vs. ra and $\bar{r}a$, where r and $\bar{r}$ are the real and imaginary parts of the wave number respectively, and a is the radius ($\kappa = a/2$). For the aluminum used, Poisson's ratio is $\nu = 0{\cdot}34$ and one thus has $E/\mu = 2{\cdot}68$. It will be assumed that the deformation is dominated by bending rather than shear and we therefore restrict our attention to the lower branch of the dispersion curve of Fig. 1. In so doing we consider

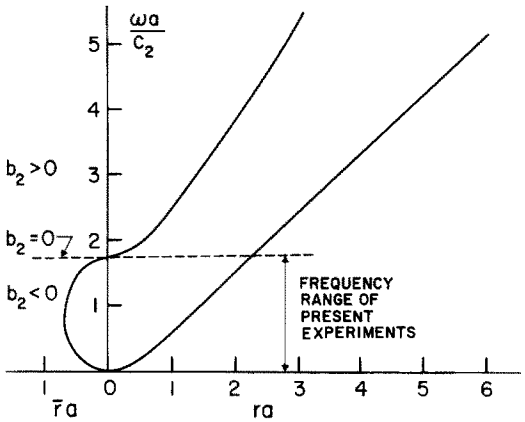

FIG. 1. Timoshenko dispersion curve for a circular elastic bar with Poisson's ratio $\nu = 0{\cdot}34$.

frequencies no higher than that corresponding to pure thickness shear motion of the beam.

As shown by Mindlin and Deresiewicz [9] the pure thickness shear frequency for a Timoshenko beam of radius a is $\omega^* = 2\lambda^{\frac{1}{2}}c_2/a$. At this frequency $b_2 = 0$ (since $\kappa = a/2$) and thus for $\omega > \omega^*$, one has $b_2 > 0$. The solution to (1) corresponding to the lower branch of the dispersion curve is thus obtained when $\omega < \omega^*$ ($b_2 < 0$).

The spatial part of the solution of interest can now be written as

$$y(x) = A_1 \exp(-irx) + A_2 \exp(irx) + A_3 \exp(-\bar{r}x) + A_4 \exp(\bar{r}x) \tag{5}$$

where

$$r = +[b_1 + (b_1^2 - b_2)^{\frac{1}{2}}]^{\frac{1}{2}} \tag{6a}$$

$$(b_2 < 0)$$

$$\bar{r} = +[-b_1 + (b_1^2 - b_2)^{\frac{1}{2}}]^{\frac{1}{2}}. \tag{6b}$$

The first two terms on the right hand side of (5) correspond to harmonic travelling waves and the last two terms correspond to exponential standing waves. In the sequel we shall refer to these as H and E waves respectively.

As indicated earlier, the parameter λ has the value 0·75 for a circular beam in static bending. Mindlin and Deresiewicz [9] deduced a dynamic value of λ by matching ω^* in the exact three dimensional (Pochhammer–Chree) and Timoshenko theories. In the exact theory $\omega^* = 1{\cdot}841\, c_2/a$ for a circular bar of radius a and in the Timoshenko theory $\omega^* = 2\lambda^{\frac{1}{2}} c_2/a$. Thus, at the pure thickness-shear frequency one has $\lambda = 0{\cdot}847$. This procedure is somewhat arbitrary, but does indicate that for $\omega < \omega^*$, λ is only a weak function of frequency. Thus, the static value should be an adequate choice over the entire frequency range of interest and this is verified in Section 3.2.

2.2 *Refraction of a flexural wave at a discontinuity in impedance*

In the next section we shall approximate a nonuniform, inhomogeneous region of a bar by a set of uniform, homogeneous elements. In preparation, we now consider the reflection and transmission of a flexural wave which is incident on the junction between two such elements.

Let the wave propagate in the positive x direction and impinge on the junction at $x = 0$ as shown in Fig. 2. The properties of the segments on the incidence and transmission side of

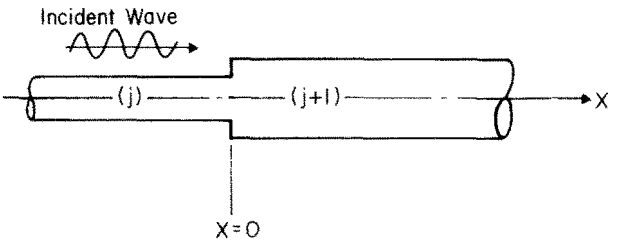

FIG. 2. Flexural wave incident on an impedance junction.

the junction are denoted by the subscripts j and $j+1$ respectively. It may be assumed for the present that the two segments are semi-infinite in length so that no free end reflections are superimposed on the refracted waves. If the incident wave is harmonic and of the form $y_j = \exp i(\omega t - r_j x)$, then from (5) the spatial parts of the solutions for the reflected and transmitted waves are

$$y_j(x) = \exp(-ir_j x) + R\exp(ir_j x) + R'\exp(\bar{r}_j x) \tag{7}$$

and

$$y_{j+1}(x) = T\exp(-ir_{j+1}x) + T'\exp(-\bar{r}_{j+1}x) \tag{8}$$

respectively.

The first term on the right hand side of (7) represents the incident harmonic wave of unit amplitude and the second term represents a reflected H (harmonic travelling) wave of amplitude R propagating in the negative x direction. The last term in (7) represents an E (exponential standing) wave of peak amplitude R' which decays with distance in the negative x direction. An additional E wave term, suggested by the complete solution (5), is

deleted in (7) by reason of the physical requirement that there not be a continuously increasing amplitude as the distance from the junction increases.

The first term on the right hand side of (8) represents a transmitted H wave of amplitude T propagating in the positive x direction. The second term represents an E wave of peak amplitude T' which decays with distance in the positive x direction. The extraneous E wave is deleted as before.

At the junction it is required that the transverse velocity, angular velocity, moment and shear force be continuous. Thus, at $x = 0$ one has

$$\begin{aligned} y_j(0) &= y_{j+1}(0) \\ y_j'(0) &= y_{j+1}'(0) \\ E_j I_j y_j''(0) &= E_{j+1} I_{j+1} y_{j+1}''(0) \\ E_j I_j y_j'''(0) &= E_{j+1} I_{j+1} y_{j+1}'''(0) \end{aligned} \tag{9}$$

where I is the moment of inertia and each prime on y denotes one differentiation with respect to x.

Substituting (7) and (8) into (9), and noting that $I = \pi a^4/4$ for a circular bar of radius a, one obtains the following set of equations for the four coefficients R, R', T and T':

$$\begin{aligned} R + R' - T - T' &= -1 \\ iR + k_1 R' + ik_2 T + k_3 T' &= i \\ -R + k_1^2 R' + \phi k_2^2 T - \phi k_3^2 T' &= 1 \\ -iR + k_1^3 R' - i\phi k_2^3 T + \phi k_3^3 T' &= -i \end{aligned} \tag{10}$$

where

$$k_1 = \bar{r}_j/r_j, k_2 = r_{j+1}/r_j, k_3 = \bar{r}_{j+1}/r_j, \phi = (E_{j+1} a_{j+1}^4)/E_j a_j^4. \tag{11}$$

The solutions for the four coefficients in terms of the parameters k_1, k_2, k_3 and ϕ are easily obtained but are algebraically complicated. They are given in the Appendix for reference.

It is necessary to convert (7) and (8) into corresponding expressions for the axial surface strains since the experimental results are obtained with strain gauges. Thus, noting that the axial surface strain ε is related to the transverse velocity y through the equation

$$\varepsilon = -\frac{a}{i\omega} y'', \tag{12}$$

one has, for the spatial part of the strain,

$$\begin{aligned} \varepsilon_j &= \frac{a_j}{i\omega}[r_j^2 \exp(-ir_j x) + r_j^2 R \exp(ir_j x) - \bar{r}_j^2 R' \exp(\bar{r}_j x)] \\ \varepsilon_{j+1} &= \frac{a_{j+1}}{i\omega}[r_{j+1}^2 T \exp(-ir_{j+1} x) - \bar{r}_{j+1}^2 T' \exp(-\bar{r}_{j+1} x)]. \end{aligned} \tag{13}$$

If the strain associated with the incident H wave, the reflected H wave, the reflected E wave, the transmitted H wave and the transmitted E wave are denoted by ε_i^H, ε_r^H, ε_r^E, ε_t^H and

ε_i^E respectively, one has from (7), (8) and (13), at $x = 0$

$$\begin{aligned} \frac{\varepsilon_r^H}{\varepsilon_i^H} &= R, & \frac{\varepsilon_r^E}{\varepsilon_i^H} &= -k_1^2 R' \\ \frac{\varepsilon_t^H}{\varepsilon_i^H} &= \frac{a_{j+1}}{a_j} k_2^2 T, & \frac{\varepsilon_t^E}{\varepsilon_i^H} &= -\frac{a_{j+1}}{a_j} k_3^2 T'. \end{aligned} \tag{14}$$

In treating the propagation of a pulse through a sequence of impedance elements it is necessary to evaluate R, R', T and T' for each relevant harmonic in the Fourier spectrum of the pulse at each impedance junction. It is thus convenient to introduce subscripts j and n for the coefficients to designate the junction number and Fourier harmonic respectively. The frequency of the nth harmonic is $n\omega_0$, where ω_0 is the base frequency of the Fourier analysis. Since we will be dealing with a sequence of impedance elements it will be convenient to adopt the following conventions: (a) elements are numbered in the direction of propagation of the original incident pulse, (b) each junction is given the same number as the lower numbered adjacent element. Thus, junction j occurs between elements j and $j+1$.

For an H wave of frequency $n\omega_0$ which is incident on junction j, as in Fig. 2, we can write (14) more compactly as:

$$\begin{aligned} \varepsilon_r^H &= Q_{jn}^H \varepsilon_i^H, & \varepsilon_r^E &= Q_{jn}^E \varepsilon_i^H \\ \varepsilon_t^H &= P_{jn}^H \varepsilon_i^H, & \varepsilon_t^E &= P_{jn}^E \varepsilon_i^H \end{aligned} \tag{15}$$

where

$$\begin{aligned} Q_{jn}^H &= R_{jn}, & Q_{jn}^E &= -k_1^2 R'_{jn} \\ P_{jn}^H &= \frac{a_{j+1}}{a_j} k_2^2 T_{jn}, & P_{jn}^E &= -\frac{a_{j+1}}{a_j} k_3^2 T'_{jn}. \end{aligned} \tag{16}$$

As a result of internal reflections, a wave can be incident on either side of a junction. When incidence occurs in the direction of increasing j, the coefficients are those of (16) and when incidence occurs in the direction of decreasing j the roles of elements j and $j+1$ are interchanged and the coefficients are distinguished by the superposed symbol $\sim$. Thus, for example $\tilde{P}_{jn}^H = a_j/a_{j+1} \tilde{k}_2^2 \tilde{T}_{jn}$, where $\tilde{k}_2 = r_j/r_{j+1}$.

In order to analyze the progress of a flexural wave through a series of impedance junctions, one must also consider the refraction problem associated with an incident E wave. The procedure is completely analogous to that for an incident H wave. The algebraic equations to be solved are identical to those in (10) except for the right hand sides where, instead of $-1, i, 1, -i$, one has $-1, k_1, -k_1^2, k_1^3$ respectively. The coefficients R, R', T and T' in (10) are replaced by $\bar{R}$, $\bar{R}'$, $\bar{T}$ and $\bar{T}'$ respectively. Solutions for these coefficients are given in the Appendix.

Following the same procedure as before we define four new coefficients

$$\begin{aligned} q_{jn}^H &= \bar{R}_{jn}, & q_{jn}^E &= -k_1^2 \bar{R}'_{jn} \\ p_{jn}^H &= \frac{a_{j+1}}{a_j} k_2^2 \bar{T}_{jn}, & p_{jn}^E &= -\frac{a_{j+1}}{a_j} k_3^2 \bar{T}'_{jn} \end{aligned} \tag{17}$$

which relate the amplitudes of the refracted strain waves to the incident E wave as follows:

$$\begin{aligned} \varepsilon_r^H &= q_{jn}^H \varepsilon_i^E, \qquad \varepsilon_r^E = q_{jn}^E \varepsilon_i^E \\ \varepsilon_t^H &= p_{jn}^H \varepsilon_i^E, \qquad \varepsilon_t^E = p_{jn}^E \varepsilon_i^E. \end{aligned} \tag{18}$$

As before, there are 4 distinct coefficients when incidence occurs in the direction of decreasing j, i.e. $\tilde{q}_{jn}^H$, $\tilde{p}_{jn}^H$, $\tilde{q}_{jn}^E$, $\tilde{p}_{jn}^E$. One thus has 16 frequency dependent coefficients governing the refraction problem at each junction.

2.3 *Propagation through a continuously variable region*

In the illustrative bar specimen of Fig. 3(a), the transition region is divided into three uniform cylindrical elements of length Δx. It is assumed that the Timoshenko beam equation (1) is the valid equation of motion in each element.

Consider a harmonic wave which propagates along the small end of the bar and is incident on the transition. At each junction a portion of the wave will be transmitted and a portion reflected. This is illustrated in Fig. 3(b) for some typical trajectories through the transition. It is readily seen that trajectories which include an even number of internal reflections lead to transmission through the transition and those which include an odd number of internal reflections lead to reflection from the transition. There is also a single direct transmission trajectory which includes no internal reflections and this is shown as trajectory $T1$ on the transmission side of the transition. As a consequence of the dispersive

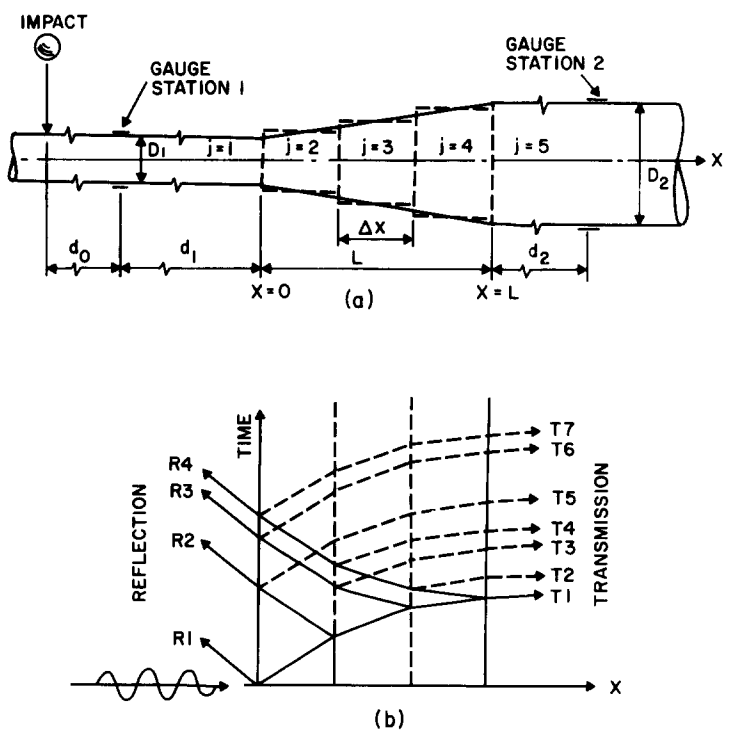

FIG. 3. (a) Schematic representation of a typical nonuniform bar. (b) Trajectories in the position–time plane.

character of flexural waves, the trajectory slopes in Fig. 3(b) change from element to element. For illustration, the slopes shown correspond to the case of a homogeneous transition in which the radius is monotonically increasing in the direction of propagation of the incident pulse.

As an illustration of the computation procedure consider the propagation of a flexural wave of angular frequency $n\omega_0$ along the direct transmission path $T1$ through the three-element transition region of Fig. 3(a). Let the incident harmonic strain wave propagate in the positive x direction and impinge on the first junction, $j = 1$, at $x = 0$. The incident wave can be represented in the form

$$\varepsilon_i^H = A_n \exp i(n\omega_0 t - r_{1n}x) \tag{19}$$

where $A_n = a_n - ib_n$ is the complex amplitude, and r_{1n} is given by (6a) for the frequency $n\omega_0$ in element 1 (the uniform segment ahead of the transition). When pulses are considered, a_n and b_n will serve as the Fourier coefficients for the nth harmonic.

In order to arrange the calculations in a suitable form for computer programming, it is convenient to accumulate the real and imaginary parts of the products of the complex coefficients separately at each junction. These can then be combined after passage through the final junction and expressed as an aggregate amplitude factor and phase shift. The computation scheme for propagation along trajectory $T1$ of Fig. 3(b) is illustrated in Fig. 4. The real and imaginary parts of each complex quantity are designated by square and wavy brackets, i.e. [ ] and { }, respectively and the decay factor for E waves in each element is denoted by $\gamma_{jn} = \exp(-\bar{r}_{jn}\Delta x)$.

At each junction the accumulated real and imaginary parts of the coefficients are designated as $[H_{jn}]$, $\{H_{jn}\}$ for H waves and $[E_{jn}]$, $\{E_{jn}\}$ for E waves. Thus, at the first junction in Fig. 4 there is an incident H wave of amplitude A_n and one has $[H_{1n}] = 1$, $\{H_{1n}\} = 0$. The coefficients of the refracted H and E waves in element 2 are separated into real and imaginary parts and the accumulated coefficients for the waves which are incident on the second junction are designated $[H_{2n}]$, $\{H_{2n}\}$, $[E_{2n}]$, $\{E_{2n}\}$ in the diagram. In the next stage the complex products are again separated into real and imaginary parts; like waves are then grouped together and are incident on junction 3. This procedure can be continued indefinitely when there are additional impedance junctions. In general the aggregate coefficients at each successive junction can be written as

$$\begin{aligned} H_{(j+1)n} &= P_{jn}^H H_{jn} + p_{jn}^H E_{jn} \\ E_{(j+1)n} &= (P_{jn}^E H_{jn} + p_{jn}^E E_{jn})\gamma_{(j+1)n} \end{aligned} \tag{20a}$$

for transmission in the direction of increasing j and

$$\begin{aligned} \tilde{H}_{(j-1)} &= \tilde{P}_{jn}^H \tilde{H}_{jn} + \tilde{p}_{jn}^H \tilde{E}_{jn} \\ \tilde{E}_{(j-1)} &= (\tilde{P}_{jn}^E \tilde{H}_{jn} + \tilde{p}_{jn}^E \tilde{E}_{jn})\gamma_{jn} \end{aligned} \tag{20b}$$

for transmission in the direction of decreasing j as indicated by the superposed $\sim$. The corresponding expressions for reflection are

$$\begin{aligned} \tilde{H}_{(j-1)n} &= Q_{jn}^H H_{jn} + q_{jn}^H E_{jn} \\ \tilde{E}_{(j-1)n} &= (Q_{jn}^E H_{jn} + q_{jn}^E E_{jn})\gamma_{jn} \end{aligned} \tag{21a}$$

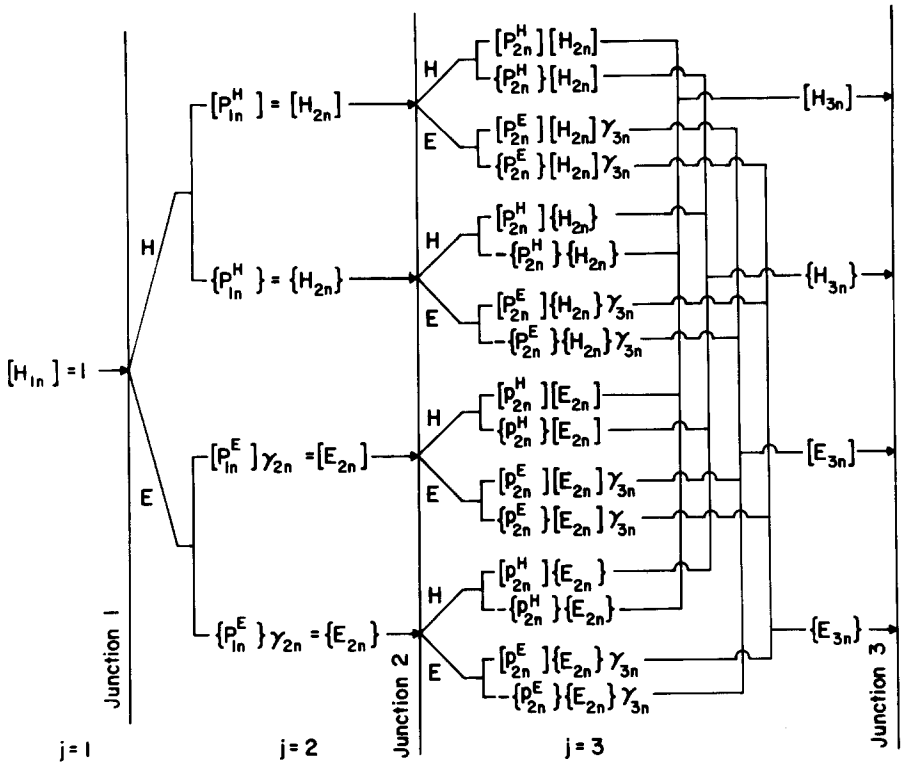

FIG. 4. Computation scheme for a sequence of transmissions.

when incidence occurs in the direction of increasing j and

$$H_{(j+1)n} = \tilde{Q}^H_{jn}\tilde{H}_{jn} + \tilde{q}^H_{jn}\tilde{E}_{jn}$$
$$E_{(j+1)n} = (\tilde{Q}_{jn}\tilde{H}_{jn} + \tilde{q}_{jn}\tilde{E}_{jn})\gamma_{(j+1)n} \tag{21b}$$

when incidence occurs in the direction of decreasing j. Equations (20a), (20b), (21a) and (21b) may be used in combination to determine cumulative coefficients along any trajectory.

Since the last step along any trajectory is a transmission through either the first or last junction, the final value of the aggregate coefficients will be obtained from (20a) or (20b). However, the exponential decay term for E waves is deleted from the coefficient after the final junction. This decay is incorporated in the representation of the wave in the uniform end section.

It is convenient to introduce special notation for the final values of the aggregate coefficients. Let these be denoted by α^H_{mn}, α^E_{mn} for the transmission trajectories, and β^H_{mn}, β^E_{mn} for the reflection trajectories. The superscripts again refer to the corresponding wave types and the subscripts m and n denote the trajectory number and Fourier harmonic respectively.

Consider now a transition region of length L which begins at $x = 0$ and terminates in two uniform, semi-infinite sections. The incidence side of the bar is regarded as the first impedance element, $j = 1$, and the transmission side is regarded as the last element denoted

by j^*. The four refracted waves emerging from the transition on trajectory m due to the incident wave (19) will be

$$\varepsilon_t^H = |\alpha_{mn}^H| A_n \exp i\{n\omega_0[t - \tau_{mn}^t - (x-L)/c_{j^*n}] + \theta_{mn}^t\}, (x \geq L) \tag{22a}$$

$$\varepsilon_t^E = |\alpha_{mn}^E| A_n \exp[-\bar{r}_{j^*n}(x-L)] \exp i[n\omega_0(t-\tau_{mn}^t) + \psi_{mn}^t], (x \geq L) \tag{22b}$$

$$\varepsilon_r^H = |\beta_{mn}^H| A_n \exp i[n\omega_0(t-\tau_{mn}^r + x/c_{1n}) + \theta_{mn}^r], (x \leq 0) \tag{22c}$$

$$\varepsilon_r^E = |\beta_{mn}^E| A_n \exp(\bar{r}_{1n}x) \exp i[n\omega_0(t-\tau_{mn}^r) + \psi_{mn}^r], (x \leq 0) \tag{22d}$$

where τ_{mn}^t and τ_{mn}^r represent the total travel time in the transition for the mth transmission and reflection trajectories respectively. These times are given by

$$\tau_{mn}^r \text{ or } \tau_{mn}^t = \sum_j \frac{\Delta x}{c_{jn}} \tag{23}$$

where the summation is carried out over all the elements traversed along the mth trajectory, inclusive of round trips where appropriate and c_{jn} is the local phase velocity given by $c_{jn} = r_{jn}/n\omega_0$. The phase angles θ_{mn}^t, ψ_{mn}^t, θ_{mn}^r, ψ_{mn}^r are the accumulated values along the mth trajectory and are given by

$$\theta_{mn}^t = \arctan\{\alpha_{mn}^H\}/[\alpha_{mn}^H], \qquad \psi_{mn}^t = \arctan\{\alpha_{mn}^E\}/[\alpha_{mn}^E] \tag{24}$$

$$\theta_{mn}^r = \arctan\{\beta_{mn}^H\}/[\beta_{mn}^H], \qquad \psi_{mn}^r = \arctan\{\beta_{mn}^E\}/[\beta_{mn}^E]. \tag{25}$$

We may now consider the refraction problem associated with an arbitrary flexural *pulse* which is incident on a transition region of variable impedance in a bar. Let the pulse propagate along one of the (semi-infinite) uniform end sections and be observed at a distance d_1 from the start of the transition [Fig. 3(a)]; the strain pulse can be represented in the form of a truncated Fourier series

$$\varepsilon_i^H(-d_1, t) = \sum_{n=0}^{N} (a_n \cos n\omega_0 t + b_n \sin n\omega_0 t). \tag{26}$$

The upper limit of summation, N, is chosen large enough to obtain the desired accuracy in representing the pulse. The coefficients a_n and b_n are determined numerically using the usual Fourier method and are thus regarded as known.

It is convenient to choose a temporal frame of reference which moves with the front of the pulse. In so doing, the pulse can be represented in the form (26) at the entrance to the transition by modifying a_n and b_n. Thus, making the substitution $t_1 = t - d_1/v$, where v is the fastest group velocity of any wave packet in the harmonic content of the pulse, the Fourier representation of the incident pulse at $x = 0$ is

$$\varepsilon_i^H(0, t_1) = \sum_{n=0}^{N} (\bar{a}_n \cos n\omega_0 t_1 + \bar{b}_n \sin n\omega_0 t_1) \tag{27}$$

where

$$\begin{aligned} \bar{a}_n &= a_n \cos n\omega_0 d_1 \left(\frac{1}{v} - \frac{1}{c_{1n}}\right) + b_n \sin n\omega_0 d_1 \left(\frac{1}{v} - \frac{1}{c_{1n}}\right) \\ \bar{b}_n &= b_n \cos n\omega_0 d_1 \left(\frac{1}{v} - \frac{1}{c_{1n}}\right) - a_n \sin n\omega_0 d_1 \left(\frac{1}{v} - \frac{1}{c_{1n}}\right). \end{aligned} \tag{28}$$

Using the real parts of (22a) and (22c), replacing a_n by $\bar{a}_n$ and b_n by $\bar{b}_n$, the refracted harmonic pulses emerging from the transition are

$$\varepsilon_t^H(x, t_2) = \sum_{n=0}^{N} \sum_{m=1}^{M^t} |\alpha_{mn}^H| \operatorname{Re}\left\{A_n \exp i\left[n\omega_0\left(t_2 - \tau_{mn}^t - \frac{(x-L)}{c_{j^*n}} + \frac{L}{v}\right) + \theta_{mn}^t\right]\right\} (x \geq L) \tag{29}$$

$$\varepsilon_r^H(x, t_1) = \sum_{n=0}^{N} \sum_{m=1}^{M^r} |\beta_{mn}^H| \operatorname{Re}\left\{\bar{A}_n \exp i\left[n\omega_0\left(t_1 - \tau_{mn}^r + \frac{x}{c_{1n}}\right) + \theta_{mn}^r\right]\right\} (x \leq 0) \tag{30}$$

where $\bar{A}_n = \bar{a}_n - i\bar{b}_n$, and $t_2 = t_1 - L/v$. The summation limits M^t and M^r correspond to the number of transmission and reflection trajectories respectively which are to be included in the calculations.

The refracted E waves which emerge from the transition are

$$\varepsilon_t^E(x, t_2) = \sum_{n=0}^{N} \exp[-\bar{r}_{j^*n}(x-L)]\left\{\sum_{m=1}^{M^t} |\alpha_{mn}^E| \operatorname{Re}\left(\bar{A}_n \exp i\left[n\omega_0\left(t_2 - \tau_{mn} + \frac{L}{v}\right) + \psi_{mn}^t\right]\right)\right\} (x \geq L) \tag{31}$$

$$\varepsilon_r^E(x, t_1) = \sum_{n=0}^{N} \exp(\bar{r}_{1n}x)\left\{\sum_{m=1}^{M^r} |\beta_{mn}^E| \operatorname{Re}(\bar{A}_n \exp i[n\omega_0(t_1 - \tau_{mn}^r) + \psi_{mn}^r])\right\} (x \leq 0). \tag{32}$$

At any position on the transmission or reflection side of the transition, the total bending strain consists of contributions from both E and H type waves. However, the contributions provided by the E waves decay exponentially with the distance from the transition. As shown in Fig. 1, the nondimensional imaginary wave number $\bar{r}a$ varies between 0·5 and 0·6 over most of the frequency range of interest. Thus, the decay factor in (31) and (32) has a value of about 0·007 at a distance of 5 diameters from the transition. Since each pair of amplitude factors $|\alpha_{mn}^H|$, $|\alpha_{mn}^E|$ and $|\beta_{mn}^H|$, $|\beta_{mn}^E|$ are of the same order, one can neglect the E wave contributions beyond a few diameters except for very low frequencies where $\bar{r}a \simeq 0$ (Fig. 1).

This property of nonpropagating flexural waves is, of course, well known and accounts for the difficulty in observing them experimentally. However, in the present case, it is possible to detect the effects of these waves indirectly by using the fact that the local contributions of the E–H interactions are accumulated in the coefficients for H waves; i.e. α_{mn}^H and β_{mn}^H. The cumulative E–H interaction can be isolated as follows: one chooses a station along each of the uniform end sections of the bar which is at least 5 diameters from the transition region so that the presence of actual E waves, given by (31) and (32) can be safely neglected. The reflected and transmitted pulse shapes are then calculated at these stations with (29) and (30) using the complete coefficients. These pulses are compared with those obtained by similar calculations using incomplete coefficients obtained by suppressing the E–H interaction. This is done by ignoring the standing wave terms in (13) or by artificially equating each E coefficient to zero throughout the calculation sequence. The difference between the results obtained is attributable to the presence of E waves generated at each impedance jump. (In the physical transition region the process is a continuous one.) Finally, the calculated pulses, with and without the E–H interaction, are compared with experiment. This procedure was carried out and is discussed in Section 3.2.

3. RESULTS

3.1 *Experimental*

Two homogeneous aluminum bars with conical transition regions were used as specimens in the experiments. Complete specimen geometries are described in Table 1 using the notation of Fig. 3(a). The distance from the impact to the first gauge station, d_0, is the same on both sides of the transition.

TABLE 1. SPECIMEN GEOMETRY: DIMENSION IN INCHES

Bar	d_0	d_1	L	d_2	D_1	D_2
1	5	15	$\frac{1}{2}$	$14\frac{1}{2}$	$\frac{1}{2}$	1
2	5	15	8	7	$\frac{1}{2}$	1

Flexural pulses were produced by the transverse impact of a $\frac{3}{8}$ in. diameter steel ball which was suspended by a fine steel wire in the configuration of a pendulum. The impact speed was carefully controlled and pulses were found to be reproducible in bars of the same diameter. The contact between ball and specimen completed a circuit for triggering a delay unit which in turn triggered a dual beam oscilloscope. The triggering delay was set slightly less than the fastest signal travel time (for flexural waves) between the impact point and the first gauge station. This time corresponds to the speed v which is the highest group velocity of flexural waves propagating in the fundamental mode; approximately equal to the shear wave speed [7], $c_2 = 3100$ m/sec in aluminum. Each of the strain gauge pairs [stations 1 and 2 in Fig. 3(a)] were connected to individual bridge circuits arranged for detecting bending strains and cancelling longitudinal strains. The output of each circuit was displayed on one trace of the oscilloscope. The uniform end sections of each bar were made long enough to preclude interference between the pulses of interest and those reflected from the free ends of the specimens.

Some typical experimental pulses are shown in Figs. 5(a)–(d). Results for a specimen having a transition length $L = 0{\cdot}5$ in. (bar 1) are shown in Figs. 5(a) and (b) for pulses incident from the small and large ends respectively. Corresponding results are shown in Figs. 5(c) and (d) for a specimen of transition length $L = 8{\cdot}0$ in. (bar 2).

The three pulses on the upper trace in Fig. 5(a) are, reading from left to right, the incident pulse, the pulse reflected from the transition, and the pulse reflected from the free end. The main parts of these pulses are well separated but the last two overlap because the reflection from the transition actually persists indefinitely. The upper trace in Fig. 5(c) shows the same incident pulse as in Fig. 5(a) but there is no discernible reflection from the transition. The free end reflection again appears at the right side of the trace.

The upper trace in Fig. 5(b) shows the incident pulse and the reflection from the transition. There is no free end reflection on this trace since the 1 in. diameter end of the bar was long enough to delay it beyond the time interval of the trace. Similarly, no free end reflection appears on the upper trace in Fig. 5(d) and, as in Fig. 5(c), there is also no detectable reflection from the transition. The lower trace in each of Figs. 5(a)–(d) shows the transmitted pulse; free end reflections are delayed beyond the trace interval.

3.2 *Numerical results*

In order to describe the net refracted waves of reflection and transmission, one must in principle account for the contribution along every trajectory of the infinite set in the

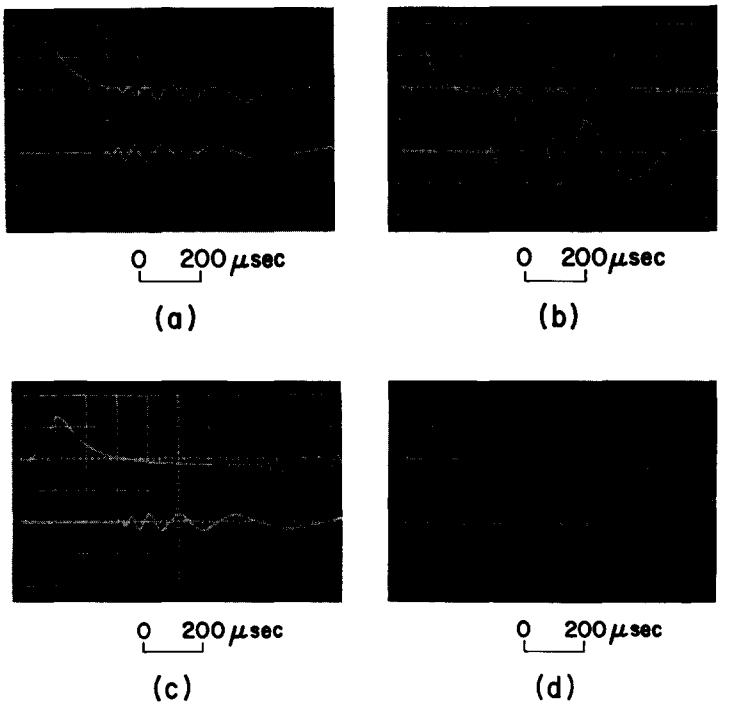

FIG. 5. Experimental strain pulses. (a) Bar 1, pulse incident from small end. (b) Bar 1, pulse incident from large end. (c) Bar 2, pulse incident from small end. (d) Bar 2, pulse incident from large end.

facing p. 1516

position–time plane. However, it is often possible to obtain adequate accuracy by considering only a relatively few significant trajectories. Thus, to illustrate the technique, we consider a simple example in which only trajectory $T1$ is used in computing the transmitted wave and only trajectories which include one internal reflection [such as $R1$, $R2$, $R3$, $R4$ in Fig. 3(b)] are used in computing the reflected wave. The number of such reflection trajectories is evidently equal to the number of impedance junctions. Thus if there are K impedance junctions in a transition region one has, for the illustrative example, $M^r = K$ and $M^t = 1$ in (29) and (30).

The degree to which such simplifications affect the accuracy of results is discussed in detail for longitudinal waves in [1], but the essential criteria apply in the present case and may be summarized as follows: if the variation in impedance along the transition is sufficiently small, and if the conditions $|Q^H_{jn}| \ll 1$ and $|P^H_{jn}| \sim 1$ obtain at each junction, then the contributions along trajectories which include the least number of internal reflections are dominant. (Typical values of these coefficients are given in the Appendix.) For example, the 6 transmission trajectories in Fig. 3(b) which include two internal reflections (shown as dashed lines $T2$–$T7$) furnish a contribution which is less than that along the direct trajectory $T1$ by a factor of approximately $6(|Q^H_{jn}|)^2$. For a transition with strong variations in impedance it will generally be necessary to expand the calculations with additional trajectories (which include more internal reflections) even if the transition is subdivided into a large number of elements. When the number of calculations required becomes very large, the utility of the present technique is however seriously compromised and in this sense is most useful when the change in impedance along the transition is not too great.

In the first stage of the calculations, it is required that the incident pulse be determined at $x = 0$ according to (27) and (28). As a check on the accuracy of the calculated input pulse, an experiment was performed in a $\frac{1}{2}$ in. diameter uniform bar over a measuring distance of 15 in., the value of d_1 in Fig. 3(a). The pulse was first detected at a distance of 5 in. from the impact point and was therefore identical to that of Figs. 5(a) and (c). Calculated results, based on (27) and (28) are compared with experiment in Fig. 6 and are in very good agreement. This also serves as *a posteriori* evidence that the static value of λ may be used in (1).

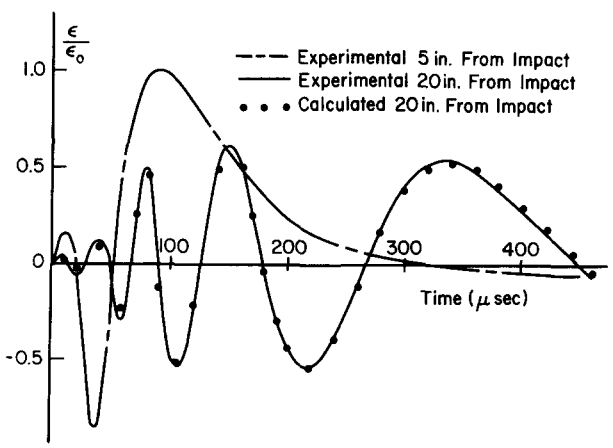

FIG. 6. Experimental and calculated pulses for propagation along a uniform $\frac{1}{2}$ in. diameter aluminum bar.

In this and subsequent calculations the fundamental frequency is $\omega_0 = 4\pi \times 10^3$ rad./sec and $N = 30$ Fourier harmonics are used to represent the pulse. The maximum value of the nondimensional frequency, corresponding to $N = 30$, is $30\omega_0 a/c_2 = 0{\cdot}773$, which is considerably less than the critical value $\omega^* a/c_2 = 1{\cdot}841$ where the higher branch of the Timoshenko dispersion curve begins (Fig. 1). The value chosen for N is, of course, arbitrary and for sufficiently large N one would have $N\omega_0 a/c_2 > 1{\cdot}841$. However, for smooth pulses, the Fourier coefficients decrease rapidly in magnitude as N increases. In the present case one has $a_{30}/a_1 < 0{\cdot}001$ and $b_{30}/b_1 < 0{\cdot}001$ so that the contribution of higher harmonics is entirely negligible.

Some typical calculated results are given in Figs. 7 and 8 at the strain gauge positions of bar 1. The amplitudes of standing waves, as given by (31) and (32), were negligible (less than

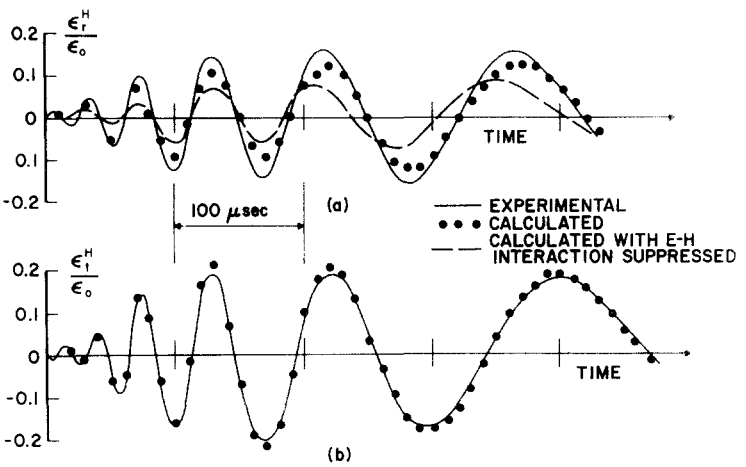

FIG. 7. Experimental and calculated results for a pulse which is incident from the small end in bar 1.

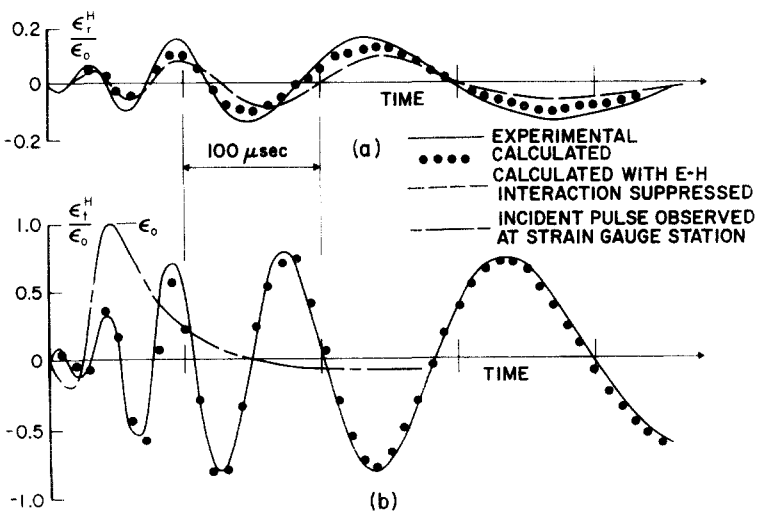

FIG. 8. Experimental and calculated results for a pulse which is incident from the large end in bar 1.

1 per cent of the propagating wave amplitudes) at the strain gauge stations and are therefore not included in the calculated pulses. At positions near the ends of the transition (within one diameter), however, the standing and propagating wave amplitudes were found to be comparable, although the latter were always greater.

The transition region of bar 1 was approximated by 16 elements ($K = 17$ junctions) and the limits on the trajectory summation in (29) and (30) were $M^t = 1$, $M^r = K = 17$. In carrying out the computations, one sets $x = d_2$ in (29), $x = -d_1$ in (30) for Fig. 7, and $x = d_1$ in (29), $x = -d_2$ in (30) for Fig. 8. Numerical evaluation of these equations is expedited by making the substitutions $t_2^* = t_2 - d_2/v$, $t_1^* = t_1 - d_1/v$ and $t_2^* = t_2 - d_1/v$, $t_1^* = t_1 - d_2/v$ in the calculations for Figs. 7 and 8 respectively. The time shifts would be introduced in (31) and (32) if one wishes to calculate the E waves.

In Fig. 7 the amplitudes of the reflected and transmitted pulses are scaled with respect to the peak amplitude, ε_0, of the incident pulse which is identical to that shown in Fig. 6. Calculated results for the transmitted pulse [Fig. 7(b)] are in good agreement with experiment and there is no significant change when the E–H interaction is suppressed. The calculated results for the reflected pulse [Fig. 7(a)] agree well with experiment, although less well than for the transmission. In view of the sensitivity of the reflected pulse shape to the transition geometry (see Fig. 5) it is to be expected that additional reflection trajectories would be required in the calculations to obtain improved results. It is of considerable interest to note, however, that the calculated results are substantially less satisfactory when the E–H interaction is suppressed in the case of the reflected pulse. It is clear that the calculated results suffer serious errors in both amplitude and phase when the cumulative contributions of the nonpropagating waves are ignored within the transition region.

Similar results are shown in Fig. 8 for bar 1 when the incident wave propagates in the opposite direction. The incident pulse shown in Fig. 8(b) is similar but not identical to that of Fig. 7(b) since the bar diameters on the incidence side of the transition are different. In each case, however, the incident pulse is detected 5 in. from the impact point.

Calculated results are not shown for bar 2, but these too were in substantial agreement with experiment. Additional experiments were performed with other bar specimens having transition lengths intermediate between bars 1 and 2. It was found that the reflected pulse amplitude diminishes rapidly as L increases, with little significant effect on the transmitted pulse.

4. CONCLUDING REMARKS

The refraction problem for a flexural pulse which is incident on a region of variable impedance in a bar has been studied by means of geometric acoustics. In the examples discussed, bending deformation was dominant over shear deformation, i.e. the significant harmonics in the Fourier spectrum of the pulses were below the frequency of pure thickness-shear motion.

The analytical procedure allows for variations in cross sectional area and material properties, but for experimental convenience, the technique has been illustrated for a homogeneous circular bar in which only the radius varied over a conical transition region. Typical calculated results were given for one bar in which the radius changed by a factor of 2 (corresponding to a factor of 16 in the moment of inertia) over the length of the transition. The calculated pulses were in good agreement with experiment even though only the dominant reflection and transmission trajectories were considered.

Experimental and calculated results show that the refracted pulse of reflection is extremely sensitive to the transition length, other factors being constant. The important parameter here is clearly the ratio Λ/L, where Λ is the wavelength measured on the incidence side of the transition. Since the wave number r is related to Λ by $r = 2\pi/\Lambda$, one finds from Fig. 1 that $\pi \leq \Lambda/a \leq 10\pi$, approximately, over the frequency range $\omega_0 \leq \omega \leq 30\omega_0$. Thus, for bar 1 $\pi \leq \Lambda/L \leq 10\pi$ and for bar 2, $\pi/16 \leq \Lambda/L \leq 10\pi/16$, approximately, when the incident pulse propagates from the small to the large end. In each case, the upper end of the range is most significant since the low frequency components are dominant in the pulse. Thus, as an order of magnitude estimate, one has $\bar{\Lambda}/L \sim 10$ in bar 1 and $\bar{\Lambda}/L \sim 1$ in bar 2, where $\bar{\Lambda}$ can be interpreted as the "effective" wavelength. Evidently, as the transition becomes more gradual with respect to the dominant pulse wavelengths, the reflection amplitude diminishes rapidly.

The amplitude of the transmitted pulse, on the other hand, depends primarily on the radii (and mechanical properties) of the terminating end sections and is relatively insensitive to the ratio $\bar{\Lambda}/L$.

The cumulative effect of nonpropagating flexural waves (E waves), which are generated at a succession of boundaries, has been observed indirectly. It was found that the cumulative E–H interaction has a significant influence on the refracted propagating pulse of reflection but not on the refracted propagating pulse of transmission.

Mathematically, nonpropagating flexural waves occur at an impedance discontinuity in order to permit the satisfaction of boundary conditions. Such waves are generally difficult to observe experimentally because they decay rapidly and are invariably superimposed on a propagating wave of larger amplitude. However the present results suggest a possible means for the study of such waves. Thus, since a region of continuously variable impedance appears to accumulate the interactive effects of E and H waves in the coefficients for the refracted waves, one can build up the refracted E wave amplitude to facilitate observation.

Some additional calculations, using (31) and (32), were carried out to investigate this. It was in fact verified that the amplitudes of refracted nonpropagating waves were comparable to those of refracted propagating waves on the reflection side of the transition within the first diameter. On the transmission side of the transition, the amplitudes of nonpropagating waves were typically 20 per cent of those for propagating waves within the first diameter.

REFERENCES

[1] M. MAO and D. RADER, Longitudinal stress pulse propagation in nonuniform elastic and viscoelastic bars. *Int. J. Solids Struct.* **6**, 519 (1970).
[2] V. V. TYUTEKIN and A. P. SHKVARNIKOV, Propagation of flexural waves in an inhomogeneous plate with smoothly varying parameters. *Soviet Phys. Acoustic.* **10**, 402 (1965).
[3] V. V. TYUTEKIN and A. P. SHKVARNIKOV, Reflection of flexural waves from an intermediate rod of variable thickness. *Soviet Phys. Acoust.* **13**, 511 (1968).
[4] A. D. PIERCE, Physical interpretation of the WKB or Eikonal approximation for waves and vibrations in inhomogeneous beams and plates. *J. acoust. Soc. Am.* **48**, 275 (1970).
[5] MUGIONO, Messungen der Reflexion von Biegewellen an Querschnittsprungen auf Staben. *Acustica* **5**, 182 (1955).
[6] E. A. RIPPERGER and H. N. ABRAMSON, Reflection and Transmission of Elastic Pulses in a Bar at a Discontinuity in Cross Section, *Proc. 3rd Midwest. Conf. on Solid Mech.* p. 135 (1957).
[7] E. A. RIPPERGER and H. N. ABRAMSON, A study of the propagation of flexural waves in elastic beams. *J. appl. Mech.* **24**, 431 (1957).

[8] S. P. TIMOSHENKO, On the correction for shear of the differential equation for transverse vibrations of prismatic bars. *Phil. Mag.* **41**, 744 (1921).
[9] R. D. MINDLIN and H. DERESIEWICZ, Timoshenko's Shear Coefficient for Flexural Vibrations of Beams, *Proc. 2nd U.S. Nat. Congr. of Appl. Mech.* p. 175 (1954).

APPENDIX

A.1 *Reflection and transmission coefficients*

$$R = \frac{1}{D}\{[(k_1k_3+k_2)(k_1^2-\phi k_3^2)(\phi k_2^2-1)]+i[\phi k_1^2k_2k_3(k_1k_3+k_2^2+k_3^2)-\phi k_1^2(k_3^3+k_1k_2^2+k_1k_3^2)$$
$$+\phi k_2(k_3^3+k_1k_2^2+k_2^2k_3)-\phi(k_1k_2^2+k_1k_3^3+k_2^2k_3)+(\phi^2k_2^2k_3^2+k_1^2)(k_1k_2-k_3)]\}$$

$$R' = \frac{1}{D}\{2k_2[\phi^2k_2^2k_3^2-1]+i[2k_3(\phi k_3^2+1)(\phi k_2^2-1)]\}$$

$$T = \frac{1}{D}\{2i[k_1(1+k_1^2)-k_3(\phi k_3^2+1)-\phi k_1k_3^2(k_1^2+k_1k_3+1)]\}$$

$$T' = \frac{1}{D}\{2k_2[\phi k_2^2(k_1^2+1)-1]+i[2k_1(1-\phi k_2^2)(1+k_1^2)]\}$$

$$\bar{R} = \frac{1}{D}\{2k_1k_3(k_1^2-\phi k_3^2)(\phi k_2^2+k_1^2)+2i[\phi k_1k_2^3k_3(\phi k_3-k_1)+k_1^3k_2(\phi k_3^2-1)]\}$$

$$\bar{R}' = \frac{1}{D}\{[(k_2+k_1k_3)(k_1^2+\phi^2k_2^2k_3^2)-\phi k_2k_3(k_3+k_1^3k_2)-\phi k_1(k_3^3+k_1k_2^3)]$$
$$+i[(\phi^2k_2k_3^2+k_1^2)(k_3-k_1k_2)+\phi k_1^2k_2k_3(k_2^2k_3+k_3^2-k_1k_3)$$
$$+\phi k_2k_3(k_2^2+k_3^2+k_2)+\phi k_1k_3^2(k_1k_3-k_1^2-1)-\phi k_1k_2^2(k_1^2+k_2+1)]\}$$

$$\bar{T} = \frac{1}{D}\{2k_1k_3(k_1^2-\phi k_3^2)(k_1^2+1)+i[2k_1(k_1^2-\phi k_3^2)(k_1^2+1)]\}$$

$$\bar{T}' = \frac{1}{D}\{i[2k_1^3(1-k_2)(k_1^2+1)-\phi k_1k_2^2(2k_1^2k_2+k_1^2+k_2+2)]\}$$

where

$$D = [(k_1k_3-k_2)(\phi k_3^2-k_1^2)(\phi k_2^2-1)]-i[\phi k_1^2k_2k_3(k_1k_3+k_2^2+k_3^2)+\phi k_1^2(k_3^3+k_1k_2^2+k_1k_3^2)$$
$$+\phi k_2(k_3^3+k_1k_2^2+k_2^2k_3)+\phi(k_1k_2^3+k_1k_3^2+k_2^2k_3)+(\phi^2k_2^2k_3^2+k_1^2)(k_1k_2+k_3)]$$

and k_1, k_2, k_3, ϕ are given by (11).

A.2 *Typical numerical values for the complete coefficients in* (16) *and* (17) *at an area discontinuity in a homogeneous aluminum bar*

$a_j = 0{\cdot}5000$ in., $a_{j+1} = 0{\cdot}4688$ in., $E_{j+1}/E_j = 1$, $\omega_0 = 4\pi \times 10^3$ rad/sec.

[ ] = real part, { } = imaginary part.

TABLE A1

n	$[P_{jn}^H]$	$\{P_{jn}^H\}$	$[P_{jn}^E]$	$\{P_{jn}^E\}$	$[Q_{jn}^H]$	$\{Q_{jn}^H\}$	$[Q_{jn}^E]$	$\{Q_{jn}^E\}$
1	1·0783	0·0001	0·0476	−0·0497	−0·0186	0·0035	−0·0450	−0·0462
5	1·0772	0·0004	0·0450	−0·0431	−0·0173	0·0035	−0·0428	−0·0487
10	1·0759	0·0007	0·0415	−0·0349	−0·0157	0·0035	−0·0398	−0·0512
15	1·0748	0·0010	0·0378	−0·0267	−0·0142	0·0034	−0·0364	−0·0528
20	1·0738	0·0011	0·0339	−0·0190	−0·0129	0·0032	−0·0328	−0·0536
25	1·0729	0·0012	0·0299	−0·0118	−0·0117	0·0029	−0·0290	−0·0533
30	1·0720	0·0012	0·0259	−0·0053	−0·0105	0·0025	−0·0252	−0·0520

TABLE A2

n	$[p_{jn}^E]$	$\{p_{jn}^E\}$	$[p_{jn}^H]$	$\{p_{jn}^H\}$	$[q_{jn}^E]$	$\{q_{jn}^E\}$	$[q_{jn}^H]$	$\{q_{jn}^H\}$
1	1·0807	0·0001	0·0488	−0·0493	−0·0148	0·0041	−0·0494	0·0514
5	1·0894	0·0004	0·0509	−0·0478	−0·0134	0·0041	−0·0640	0·0735
10	1·1009	0·0007	0·0531	−0·0454	−0·0119	0·0040	−0·0875	0·1134
15	1·1134	0·0010	0·0545	−0·0423	−0·0105	0·0038	−0·1190	0·1733
20	1·1274	0·0012	0·0549	−0·0387	−0·0092	0·0035	−0·1614	0·2635
25	1·1436	0·0013	0·0540	−0·0344	−0·0081	0·0032	−0·2190	0·4008
30	1·1634	0·0013	0·0512	−0·0293	−0·0071	0·0027	−0·2989	0·6140

(*Received* 8 *September* 1970)

Абстракт—Определяется непосредственный численный метод для анализа отображения волны изгиба, падающей в конечной области механического сопротивления в упругом стержне. Эта область приближена системой элементов одномерного сопротивления, рассматрыаемых в смвсле балки Тимошенки, к которым применяются методы геометрической акустики. Анализ приводится для бесконечного ряда гаронической волны и применяется далее, для случая импульса в смысле численного синтеза. Фурье. Получаются численные результаты для некоторых примеров, для которых произведены эксперименты. Определенные импульсы оказываются точно согласованными с наблюдаемываемы экспериментально. Оказывается, что содействие непрерывности взаимодействия между распространяющимися и нераспространяющимися волнами аккумулируется внутри неодноооднй области и может значительно влиять на систему импульсов ирочесса перехода и отображения.